Available online at www.sciencedirect.com
SCIENCE DIRECT
International Journal of Fatigue 28 (2006) 366–374
International Journal of Fatigue
www.elsevier.com/locate/ijfatigue

# Fatigue initiation in fibre metal laminates

J.J. Homan*

*Faculty of Aerospace Engineering, Delft University of Technology, P.O. Box 5058, 2600 GB Delft, The Netherlands*

Received 8 September 2004; received in revised form 7 June 2005; accepted 14 July 2005
Available online 6 September 2005

**Abstract**

It is assumed that fatigue crack initiation in Fibre Metal Laminates is determined by the stress cycles in the metal layers only. It is further assumed that if the stress cycles in the metal layers are known, the fatigue initiation life can be established using *S–N* data available for the given metal alloy.

The internal stresses in the aluminium layers of a Fibre Metal Laminate are different from the applied stresses on the laminate because of differences in stiffness and coefficient of thermal expansion between the metal and fibre layers. The difference in thermal expansion will cause residual stresses during cooling down after the curing process of the laminate. Classical laminate theory can be applied to calculate the internal stresses. Additional elastic considerations have led to accounting for the effect of anisotropy on the stress concentration factor.

Validation fatigue tests on Glare 3-3/2-0.3, Glare 4B-3/2-0.3 and monolithic aluminium 2024-T3 showed that the above assumptions proved to be correct. The tests showed also that the effect of off-axis loading could be predicted with the classical laminate theory.

Further, is has been shown that exposure to high temperature (70 °C) and humidity (85%) for 3000 h prior to testing has no effect on the fatigue initiation properties of Glare 3-3/2-0.3.


*Keywords:* Fibre metal laminates; Fatigue; Initiation; Stress concentration factors

## 1. Introduction

Fibre Metal Laminates (FML's) [1–3] such as Glare offer significant improvements compared to current applied materials for aircraft structures. Weight reduction and improved damage tolerance characteristics are two of the main advantages of FML's, especially for application in aircraft fuselage structures. The laminates consist of alternating thin metal alloy layers (0.2–0.5 mm) and prepregs of unidirectional fibre layers embedded in an adhesive system. These prepregs can be laid-up in different orientations.

Fibre Metal Laminates owe their good crack growth resistance to the fibres between the aluminium layers [4]. These fibres, which remain unbroken during fatigue crack growth in the aluminium layers, restrain the crack opening in the wake of the fatigue crack, as demonstrated in Fig. 1.

* Tel.: +31 15 2788230; fax: +31 15 2781151.
*E-mail address:* j.j.homan@lr.tudelft.nl

0142-1123/$ - see front matter © 2005 Elsevier Ltd. All rights reserved.
doi:10.1016/j.ijfatigue.2005.07.030

If the fibres were not present, the remote stress must be transferred around the crack in the metal layer. The presence of the fibres implies that a part of the load is transferred through the fibres in the wake of the crack. Additionally, the fibres cause a restraint on the crack tip opening. Due to loading the crack in the aluminium layer tend to open. The fibres in the wake of the crack will be elongated but because of their stiffness this elongation is limited [4]. Both effects lead to a considerable reduction of the stress intensity factor and hence a very low crack growth rate. This is illustrated in Fig. 2.

During the initiation phase and the first part of the crack growth phase, the crack bridging mechanism is still not present. Research by Alderliesten [5] showed that the fibres become fully effective from a crack length varying between some tenth of a millimetre to a few millimetres, depending on the laminate. It is also the order of magnitude for metals at which a transition from micro crack growth to macro crack growth occurs. After this transition, the laws of linear elastic fracture mechanics become applicable, whereas micro crack nucleation and the initial crack growth are determined by surface conditions and stress concentrations. Different phases of the fatigue life in Fibre Metal Laminates together with relevant factors are illustrated in Fig. 3.

**Notation**

| | |
|---|---|
| $a$ | angularity of a laminate |
| $C_{ij}$ | compliance matrix |
| $E$ | Young's modulus (MPa) |
| $E_{Al}$ | Young's modulus of aluminium (MPa) |
| $E_{f,0}$ | Young's modulus of prepreg in fibre direction (MPa) |
| $E_{f,90}$ | Young's modulus of prepreg perpendicular to fibre direction (MPa) |
| $E_{lam}$ | Young's modulus of complete laminate (MPa) |
| $G$ | shear modulus MPa |
| $K_t$ | stress concentration factor |
| $M$ | off-axis matrix |
| $M^T$ | transposed off-axis matrix |
| $N$ | fatigue life cycles |
| $N_f$ | fatigue life to failure cycles |
| $N_i$ | fatigue initiation life cycles |
| $N_{0.1}$ | fatigue initiation life to a crack length of 0.1 mm cycles |
| $p$ | layer |
| $r$ | directionality of a laminate |
| $R$ | stress ratio |
| $S$ | stress (MPa) |
| $S$ | stiffness matrix |
| $t_{Al}$ | total thickness of the aluminium layers in a laminate (mm) |
| $t_{f,0}$ | total thickness of prepreg layers with fibres in the loading direction (mm) |
| $t_{f,90}$ | total thickness of prepreg layers with fibres perpendicular to the loading direction (mm) |
| $t_{lam}$ | total thickness of a laminate (mm) |
| $T_c$ | curing temperature (°C) |
| $T_{env}$ | temperature of environment (°C) |
| $\alpha_{Al}$ | coefficient of thermal expansion of aluminium (1/°C) |
| $\alpha_{f,0}$ | coefficient of thermal expansion of prepreg in fibre direction (1/°C) |
| $\alpha_{f,90}$ | coefficient of thermal expansion of prepreg perpendicular to fibre direction (1/°C) |
| $\gamma$ | shear angle (rad) |
| $\varepsilon$ | strain |
| $\varepsilon$ | strain vector |
| $\sigma$ | stress (MPa) |
| $\sigma$ | stress vector |
| $\tau$ | shear stress (MPa) |
| $\upsilon$ | Poisson's ratio |
| $\phi$ | off-axis angle (rad) |
| $\theta$ | angle along the hole in a sheet (rad) |

It should, however, be noted that there is no physical relation between the crack length at which there is a transition from micro crack growth to macro crack growth and the crack length at which the fibres become effective.

Fig. 4 shows the contributions of each phase to the total fatigue life for both monolithic aluminium and Fibre Metal Laminates. The differences in contributions are remarkable and characteristic for these materials. The fatigue life of monolithic aluminium consists mainly of the crack initiation phase, because crack propagation is very fast and covers only a few percent of the fatigue life. The fatigue life of Fibre Metal Laminates, on the other hand, consists mainly of the crack propagation phase.

Since fatigue initiation affects only the aluminium layers (the fibre layers remain intact), the initiation process will be considered as a fatigue process in aluminium.

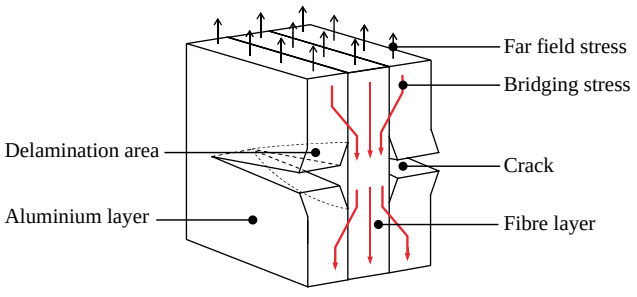


Fig. 1. Crack bridging of the fibres and delamination of the layers.

The consequence of this assumption is that the initiation life of Fibre Metal Laminates can directly be read from $S$–$N_i$ curves (e.g. from handbooks) of the constituent metal alloy, i.e. $(N_i)_{FML} = (N_f)_{Metal}$. It is the objective of this research to show that this assumption is correct.

Early research, using $S$–$N_f$ curves of metals, showed already that this assumption gives good results. However, to establish the fatigue initiation life in this way, two important aspects should be taken care of:

1. Contribution of fatigue initiation to total fatigue life.
2. The actual stress levels in the metal layers.

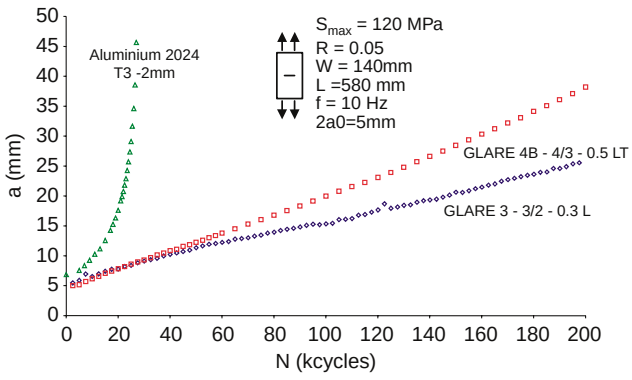


Fig. 2. Crack growth curves of aluminium 2024-T3, Glare 3-3/2-0.3 L and Glare 4B-4/3-0.5 LT for constant amplitude fatigue loading [3].

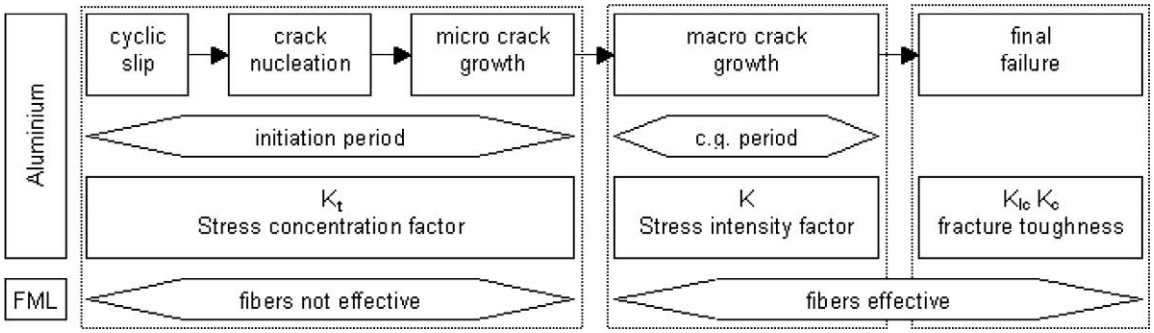


Fig. 3. Different phases of the fatigue life in Fibre Metal Laminates together with relevant factors.

Very often, the fatigue initiation life of metals is estimated using $S$–$N_f$ curves from different sources (e.g. handbooks). As already indicated in Fig. 4, the fatigue initiation life $N_i$ of Fibre Metal Laminates cannot be estimated using the total fatigue life $N_f$. Since crack growth is so slow, the initiation life is only a relatively small part of the fatigue life, even in small coupon specimens. Therefore, the assumption made for metals that $N_i$ is about the same as $N_f$ cannot be made for Fibre Metal Laminates.

Since Fibre Metal Laminates are cured at elevated temperatures, residual stresses will be present after cooling down to RT in all layers of the cured laminate, due to differences in coefficients of thermal expansion. In the aluminium layers of Glare the residual stresses are tensile stresses. Furthermore, the different layers have a different stiffness. Layers with a larger stiffness attract more load during a fatigue load cycle. In case of Glare, the aluminium layers have the highest stiffness, so these layers will have a more severe stress level. As can be seen in Fig. 5, the stress amplitude and the mean stress level are higher than those of the applied stress. Consequently, the fatigue initiation life of Glare will be shorter than that of the constituent aluminium alloy loaded with the same applied stress level.

Fatigue initiation in Fibre Metal Laminates with respect to the aspects mentioned above has been investigated. In this paper the results of this investigation are summarized. Other aspects that are addressed in this investigation are:

- Stress concentration factors.
- Effect of moisture and temperature.

## 2. Fatigue crack initiation modelling

As mentioned before, the initiation process in FML's will be considered as a fatigue process in aluminium. To be able to read the initiation lives of FML's from an $S$–$N$ curve, the actual stress cycle in the aluminium layers must be known. For the calculation of these stresses the classical laminate theory has been applied since this theory enables the determination of stresses in each layer irrespective of applied load and loading direction.

### 2.1. Aluminium stresses according to classical laminate theory

Although there are many publications dealing with the classical laminate theory, such as [7], the derivation for FML's is summarized below for clarity.

#### 2.1.1. Stresses and strains per layer

Generalized Hooke's Law:

$$\bar{\sigma} = S\bar{\varepsilon} \tag{1}$$

$$\bar{\varepsilon} = C\bar{\sigma} \tag{2}$$

where:

$$\bar{\sigma} = \begin{bmatrix} \sigma_x \\ \sigma_y \\ \tau_{xy} \end{bmatrix} \tag{3}$$

$$\bar{\varepsilon} = \begin{bmatrix} \varepsilon_x \\ \varepsilon_y \\ \gamma_{xy} \end{bmatrix} \tag{4}$$

The coordinates $x$ and $y$ coincides with the material principles axes. The compliance matrix can be written as:

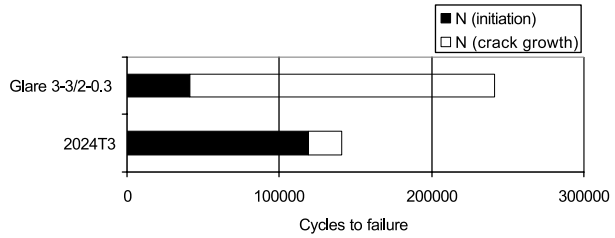


Fig. 4. Contributions of different phases to the total fatigue life in Glare 3-3/2-0.3 and 2024T3 for an open hole specimen and fatigue load as shown in Fig. 2.

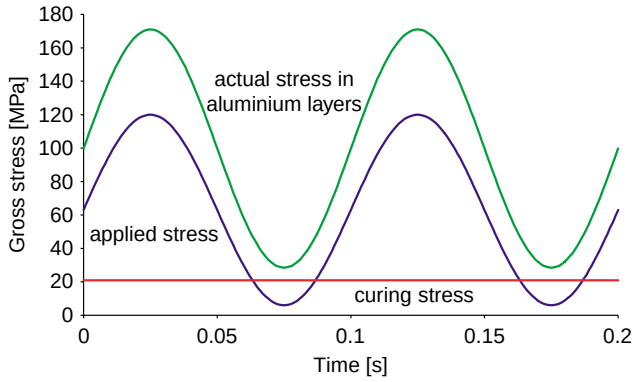


Fig. 5. The stress cycle in the aluminium layers of a Glare 3-3/2-0.3 laminate loaded in $L$ direction at RT is a superposition of the stress cycle induced by the applied stress and the curing stress [6].

$$C = \begin{bmatrix} \frac{1}{E_x} & \frac{-\upsilon_{xy}}{E_x} & 0 \\ & \frac{1}{E_y} & 0 \\ & & \frac{1}{G_{xy}} \end{bmatrix} \tag{5}$$

and the stiffness matrix can be written as:

$$S = \begin{bmatrix} \frac{E_x}{1-\upsilon_{xy}\upsilon_{yx}} & \frac{\upsilon_{xy}E_y}{1-\upsilon_{xy}\upsilon_{yx}} & 0 \\ & \frac{E_y}{1-\upsilon_{xy}\upsilon_{yx}} & 0 \\ & & G_{xy} \end{bmatrix} \tag{6}$$

The stiffness properties under angle $\phi$ are:

$$\bar{\sigma}_\varphi = M\bar{\sigma} \tag{7}$$

$$\bar{\varepsilon} = M^{\mathrm{T}}\bar{\varepsilon}_\varphi \tag{8}$$

where $M$ is the off-axis matrix:

$$M = \begin{bmatrix} m^2 & n^2 & 2mn \\ n^2 & m^2 & -2mn \\ -mn & mn & m^2-n^2 \end{bmatrix} \tag{9}$$

$$m = \cos\varphi \tag{9a}$$

$$n = \sin\varphi \tag{9b}$$

The stiffness and compliance matrix for laminates under an angle $\phi$ with respect to the material principle axes follow from:

$$\bar{\sigma}_\varphi = M\,S\,M^{\mathrm{T}}\bar{\varepsilon}_\varphi = S_\varphi\bar{\varepsilon}_\varphi \qquad S_\varphi = M\,SM^{\mathrm{T}} \tag{10}$$

$$\bar{\varepsilon}_\varphi = [M^{-1}]^{\mathrm{T}}\,CM^{-1}\bar{\sigma}_\varphi = C_\varphi\bar{\sigma}_\varphi$$
$$C_\varphi = [M^{-1}]^{\mathrm{T}}\,CM^{-1} \tag{11}$$

The inverse matrix of $M$ can be written as:

$$M^{-1} = \begin{bmatrix} m^2 & n^2 & -2mn \\ n^2 & m^2 & 2mn \\ mn & -mn & m^2-n^2 \end{bmatrix} \tag{12}$$

### 2.1.2. Stresses and strains per layer in complete laminates

Properties for layer p:

$$(\bar{\sigma}_\varphi)_p = (M^{-1})_p\bar{\varepsilon}_\varphi \tag{13}$$

Standard FML grades are defined such that the angle $\phi$ is the same for each layer.

Properties for $n$ layers:

$$(\bar{\sigma}_\varphi)_{\mathrm{lam}} = \sum_{p=1}^{n}(\bar{\sigma}_\varphi)_p\frac{t_p}{t_{\mathrm{lam}}} = \sum_{p=1}^{n}\left\{(S_\varphi)_p\frac{t_p}{t_{\mathrm{lam}}}\right\}\bar{\varepsilon}_\varphi = (S_\varphi)_{\mathrm{lam}}\bar{\varepsilon}_\varphi \tag{14}$$

The stiffness and compliance matrix for the laminate can then be written as:

$$(S_\varphi)_{\mathrm{lam}} = \sum_{p=1}^{n}(S_\varphi)_p\frac{t_p}{t_{\mathrm{lam}}} \tag{15}$$

$$(C_\varphi)_{\mathrm{lam}} = \sum_{p=1}^{n}(C_\varphi)_p\frac{t_p}{t_{\mathrm{lam}}} \tag{16}$$

### 2.1.3. Curing stresses

Cooling down from the curing temperature will cause a strain in the laminate. All individual layers must comply with this strain. This leads to the following equilibrium

$$\sum_{p=1}^{n}(S_\varphi)_p t_p\bar{\alpha}_p = (S_\varphi)_{\mathrm{lam}}t_{\mathrm{lam}}\bar{\alpha}_{\mathrm{lam}} \tag{17}$$

with $\alpha_p$ being the vector with the thermal expansion coefficient for layer p:

$$\bar{\alpha}_p = \begin{bmatrix} \alpha_x\cos(\varphi)+\alpha_y\sin(\varphi) \\ \alpha_x\sin(\varphi)+\alpha_y\cos(\varphi) \\ 0 \end{bmatrix} \tag{18}$$

Then for the laminate:

$$\bar{\alpha}_{\mathrm{lam}} = \frac{1}{t_{\mathrm{lam}}}(S_\varphi)^{-1}_{\mathrm{lam}}\sum_{p=1}^{n}(S_\varphi)_p t_p\bar{\alpha}_p \tag{19}$$

The strain due to thermal expansion is:

$$\bar{\varepsilon}_c = \bar{\alpha}_{\mathrm{lam}}\Delta T \tag{20}$$

where:

$$\Delta T = T_{\text{env}} - T_{\text{c}} \tag{21}$$

Internal stresses per layer due to curing:

$$\bar{\sigma}_{\text{c},p} = (S_\varphi)_p(\bar{\varepsilon}_{\text{c}} - \Delta T\bar{\alpha}_p) \tag{22}$$

*2.1.4. Internal stresses due to external stresses*

Assume an external stress $\sigma$:

$$\bar{\sigma} = (\bar{\sigma})_{\text{lam}} \tag{23}$$

The strain can then be written as:

$$\bar{\varepsilon} = (S_\varphi)^{-1}_{\text{lam}}(\bar{\sigma})_{\text{lam}} \tag{24}$$

The stress level in layer p will then be:

$$(\bar{\sigma}_\varphi)_p = (S_\varphi)_p\bar{\varepsilon} = (S_\varphi)_p(S_\varphi)^{-1}_{\text{lam}}(\bar{\sigma})_{\text{lam}} \tag{25}$$

*2.1.5. Summary*

The total stress level in layer p is the sum of the curing stress and the stress due to external loading. This stress level can now be written as:

$$(\bar{\sigma}_\varphi)_p = (S_\varphi)_p[(S)^{-1}_{\text{lam}}(\bar{\sigma})_{\text{lam}} + \Delta T(\alpha_{\text{lam}} - \alpha_p)] \tag{26}$$

The stiffness matrices can be derived from section *a*. for layer p and from section b. for the complete laminate. The thermal expansion coefficients can be derived from section c. The values $(\sigma)_{\text{lam}}$ and $\Delta T$ are input parameters.

Note that for Glare Eq. (15) can be rewritten as:

$$(S_\varphi)_{\text{lam}} = (S_\varphi)_{\text{Al}}\frac{t_{\text{Al}}}{t_{\text{lam}}} + (S_\varphi)_{f,0}\frac{t_{f,0}}{t_{\text{lam}}} + (S_\varphi)_{f,90}\frac{t_{f,90}}{t_{\text{lam}}} \tag{27}$$

## 2.2. Stress concentration factors

The stress concentration factor caused by a circular hole in a laminate of infinite dimensions loaded with a plane stress system can be expressed as a function of the angularity and the directionality of that laminate. The angularity and directionality are written as follows.

$$\text{Angularity}: \; a = \frac{c_{12} + \frac{c_{66}}{2}}{c_{11}} \tag{28}$$

$$\text{Directionality}: \; r = \sqrt{\frac{c_{22}}{c_{11}}} \tag{29}$$

Values for $c_{11}$, $c_{12}$, $c_{22}$ and $c_{66}$ follow from the compliance matrix for the laminate, Eq. (16):

$$(C_\varphi)_{\text{lam}} = \begin{vmatrix} c_{11} & c_{12} & 0 \\ c_{21} & c_{22} & 0 \\ 0 & 0 & c_{66} \end{vmatrix} \tag{30}$$

According to [7], the stress concentration is now written as a function of angle $\theta$ along the edge of the hole:

$$K_{\text{t}}(\theta) = \frac{r(m^2(r + \sqrt{2(r+a)}) - n^2)}{n^4 + 2am^2n^2 + r^2m^4} \tag{31}$$

where $m = \cos(\theta)$ and $n = \sin(\theta)$.

For a unidirectional load, the highest stress concentrations will be found at $\theta = 0°$. For $\theta = 0°$ Eq. (31) can be simplified to:

$$K_t = 1 + \frac{\sqrt{2(r+a)}}{r} \tag{32}$$

For an isotropic material like aluminium, $a = 1$ and $r = 1$ and therefore, $K_t = 3$.

It is now proposed that any stress concentration in a finite width fibre metal laminate sheet can be described with the following factor:

$$K_{t,\text{FML}} = \left(\frac{K_{t,\text{FML}}}{K_{t,\text{Al}}}\right)_{\text{open hole, infinite sheet}} K_{t,\text{Al}} \tag{33}$$

With Eq. (32) and $K_{t,\text{Al}} = 3.0$ for an open hole in an infinite sheet this gives:

$$K_{t,\text{FML}} = \left(\frac{K_{t,\text{Al}}}{3}\right)\left(1 + \frac{1}{r}\sqrt{2(r+a)}\right) \tag{34}$$

The peak stress at an arbitrary notch in a Fibre Metal Laminate would then be:

$$(\bar{\sigma})_{\text{lam,peak}} = K_{t,\text{FML}}(\bar{\sigma})_{\text{lam}} \tag{35}$$

For a single layer, using Eq. (26), the peak stress at a notch can be written as:

$$(\bar{\sigma}_\varphi)_p = (S_\varphi)_p[K_{t,\text{FML}}(S)^{-1}_{\text{lam}}(\bar{\sigma})_{\text{lam}} + \Delta T(\bar{\alpha}_{\text{lam}} - \bar{\alpha}_p)] \tag{36}$$

So, for a single layer, the stress concentration factor caused by a unidirectional load in $x$ direction can now be expressed as:

$$K_{t,p} = \frac{(\sigma_{\varphi,x})_{p,\text{peak}}}{(\sigma_{\varphi,x})_p} \tag{37}$$

$(\sigma_{\phi,x})_{p,\text{peak}}$ and $(\sigma_{\phi,x})_p$ follow from Eqs. (36) and (26)

In Fibre Metal Laminates, this $K_{t,p}$ is equal for each aluminium layer.

## 2.3. Estimation of fatigue life

With the equations derived above and the mechanical and physical properties of the constituents of a Fibre Metal Laminate (see Table 1 for Glare) the stresses in the metal layers can be calculated.

From the calculated stress cycles for the aluminium layers the fatigue life can be estimated using the assumption that $S$-$N_{\text{f}}$ data from the literature can be applied for the life-to-small-crack-initiation, despite the fact that these data are very often life-to-failure data.

Table 1
Mechanical and physical properties of Glare constituents

| | Al 2024-T3 | S2-glass, FM94 adhesive | |
|---|---|---|---|
| | | 0° | 90° |
| $E$ [MPa] | 72,400 | 48,900 | 5500 |
| $G$ [MPa] | 27,600 | 5550 | |
| $\upsilon_{xy}$ | 0.33 | 0.33 | |
| $\upsilon_{yx}$ | | 0.0371 | |
| $\alpha$ [1/°C] | $22\times10^{-6}$ | $6.1\times10^{-6}$ | $26.2\times10^{-6}$ |
| $T_c$ [°C] | | 120 | |
| Single prepreg layer thickness [mm] | | 0.133 | |

Note that the stress cycle is determined by calculating both the maximum and the minimum stress level separately.

The method allows the prediction of $N_i$ of Glare for each temperature for which $S$–$N_f$ curves for aluminium are available. The effect of the temperature on the internal stress levels of the aluminium layers is incorporated in the method.

## 3. Experimental data

Establishing the fatigue initiation by tests is different for FML's than for monolithic aluminium: As already illustrated in Fig. 4, the initiation life $N_i$ in FML's is much smaller than $N_f$, whereas, in monolithic aluminium $N_i$ is very close to $N_f$. For monolithic aluminium it is, therefore, common practice to establish $N_i$ by finding $N_f$. For FML's, the actual initiation life must be determined. During experiments, crack initiation life was defined as cycles to a given (small) crack length. In the present discussion, this crack length is set to 1.0 mm.

### 3.1. Un-notched specimens

Comparative fatigue tests on aluminium and Glare were performed on flat dog-bone specimens with a very low stress concentration factor of $K_t \approx 1.06$ in monolithic aluminium (see Fig. 6). The fatigue initiation tests on Glare 3-3/2-0.3 (see Table 2) were performed at different stress levels and with a stress ratio of $R=0.05$. The fatigue initiation tests on 2024-T3 1.6-mm thick specimens were performed at stress levels corresponding with the stress levels in the aluminium layers of the Glare specimens. The stress ratios for the aluminium specimens were in the range from 0.10 to 0.14.

The determination of the crack initiation was done by visual observations. At first it was planned to use four crack detection gauges. The gauges were bonded on the outer surfaces at 0.5 mm from the edges, implying that in Glare only crack initiation in the surface layers could be monitored. However, the crack wires failed long before a fatigue crack initiated.

Because the Glare specimens were visually inspected periodically instead of continuously, there was some scatter in the crack lengths at detection. Testing was stopped after detection of the first crack. The aluminium specimens were tested to failure because else very short inspection intervals were required.

Fig. 7 shows the $S$–$N$ data for the aluminium ($N_f$) and the Glare specimens ($N_i$). The fatigue initiation lives of the Glare specimens are substantially shorter than those of the aluminium specimens if compared on the basis of the overall applied stresses. However, when the comparison is made based on the stresses in the aluminium layers of the Glare laminates, the fatigue initiation lives are almost similar. The slight difference that still exists can be associated with the fact that for the aluminium specimens the fatigue to failure lives ($N_f$) are plotted, that a different thickness is used for the monolithic aluminium specimens and that some scatter will always be present.

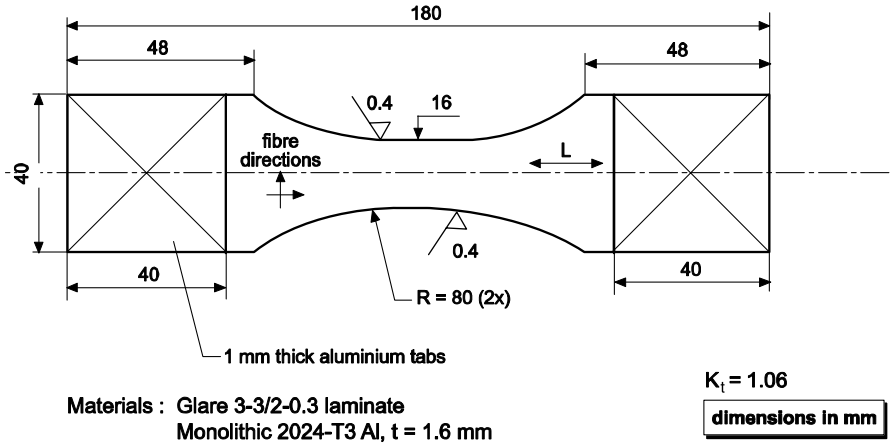


Fig. 6. Un-notched fatigue specimen.

Table 2
Glare lay-ups used for testing

| | Glare 3-3/2-0.3 | Glare 4B-3/2-0.3 |
|---|---|---|
| Number of Al layers | 3 | 3 |
| Thickness of a single Al layer (mm) | 0.3 | 0.3 |
| Single prepreg layer built-up | 0/90° | 90/0/90° |
| Single prepreg layer thickness (mm) | 0.266 | 0.399 |
| Total thickness | 1.43 | 1.70 |

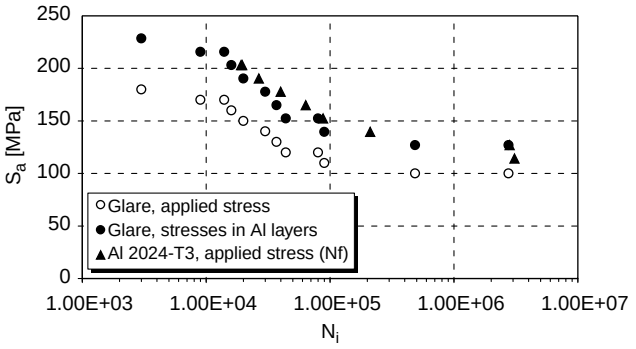


Fig. 7. Comparison of fatigue initiation lives between Glare 3-3/2-0.3 and 2024-T3 un-notched specimens at RT. Stresses in Glare are related to the overall applied stresses as well as to the stresses in the aluminium layers.

### 3.2. Effect of stress concentrations

Comparative tests were performed on flat specimens with a centre hole (Fig. 8). In monolithic aluminium, the stress concentration factor in the specimen is $K_t = 2.7$. Materials tested were Glare 3-3/2-0.3 and aluminium 2024-T3. The aluminium specimens were laminated from three layers of 0.3 mm.

Stress levels for the fatigue tests were selected similar as for the tests on the un-notched specimens. Tests were performed with a stress ratio of $R = 0.05$.

The determination of the crack initiation has been done by using the DC potential drop method. The current input and potential measuring wires were attached to the specimens with an electrically conducting adhesive. Spot welding could not be applied since this would lead to early initiation at the welds. Only the surface layers were instrumented, so only crack initiation in the surface layers could be monitored.

In Fig. 9 the $S$–$N_i$ data for the aluminium and the Glare specimens are presented. Just as for the un-notched specimens, the fatigue initiation lives of the Glare specimens are systematically lower than those of the aluminium specimens if compared on the basis of the overall applied stresses. However, the comparison based on the stresses in the aluminium layers indicated that the Glare specimens show longer initiation lives than aluminium specimens.

For sure scatter will play a role in here but it is also thought that this can be caused by the effect of anisotropy of Glare on the stress concentration factor. With Eqs. (32) and (34) the stress concentration factor for Glare 3-3/2-0.3 in the notched fatigue specimen is $K_t = 2.77$. The stress concentration factor for an aluminium layer in Glare follows from Eq. (37). According to this equation the stress concentration factor depends on the applied load and the test temperature. Since calculations are assumed to be in the elastic range, the factor is established for the case that the stress level at the notch is just below yield. Selecting an applied stress level of the aluminium yield strength divided by 3 can approach this. With an applied stress of 150 MPa, the stress concentration factor in an aluminium layer in Glare 3-3/2-0.3 will then be $K_t = 2.61$. This factor is lower than the factor in the monolithic specimens. To improve the comparison between the Glare and aluminium specimens it is decided to multiply the stress levels in the aluminium layers of the Glare specimens with a factor of 2.61/2.7 to account for the difference in stress concentration factors. The results of this comparison are given in Fig. 10. Since the ratio of 2.61/2.7 is very close to 1.0, Fig. 10 shows almost no difference

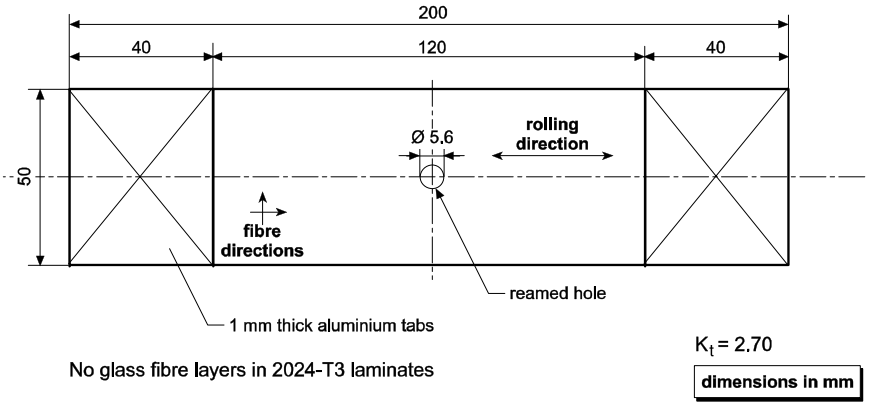


*Glare 3-3/2-0.3 and 2024-T3 laminate specimens used in fatigue crack initiation tests on notched specimens*

Fig. 8. Notched fatigue specimen.

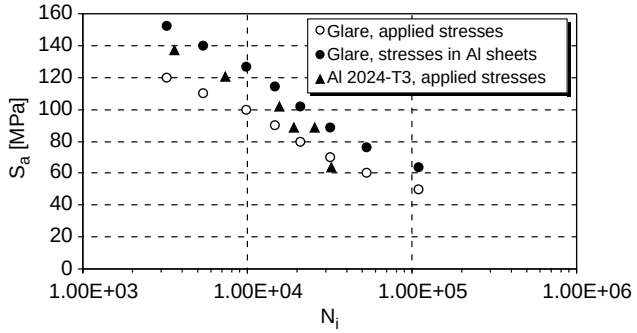


Fig. 9. Comparison of fatigue initiation lives between Glare 3-3/2-0.3 and 2024-T3 notched specimens at RT. Stresses in Glare are related to the overall applied stresses as well as to the stresses in the aluminium layers.

between the data points with and without correction for the $K_t$, although the corrected data points come closer to the data points for monolithic aluminium.

### 3.3. Off-axis loading

Fatigue tests were performed on notched specimens with a hole as shown in Fig. 8. In monolithic aluminium, the stress concentration factor in this specimen is $K_t = 2.7$. Tests were done on specimens made of Glare 4B-3/2-0.3 (see Table 2) with different angles (0, 22.5 and 45 °) between the loading direction and the rolling direction of the aluminium layers in the Glare laminates. Since aluminium 2024 shows very little anisotropy compared to fibre reinforced materials, only the effect of off-axis loading in FML's was investigated. Stress levels for the fatigue tests were selected similar as for the previous test series, again with a stress ratio of $R = 0.05$. Comparison is made with the test data of monolithic aluminium notched specimens.

Crack initiation has been determined with the same method as for the Glare 3-3/2-0.3 notched specimens discussed before.

In Fig. 11 the $S$–$N_i$ data for the aluminium and the Glare specimens are presented. Just as for the previous test series, the fatigue initiation lives of the Glare specimens are

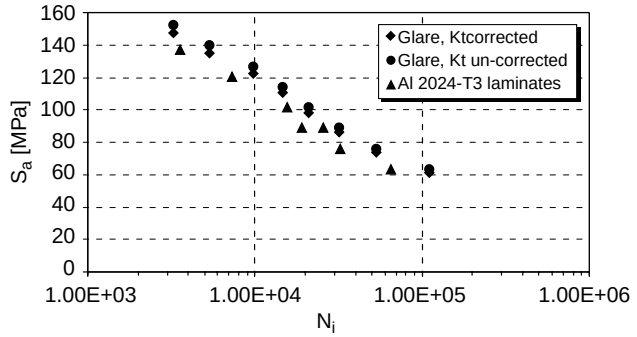


Fig. 10. Comparison of fatigue initiation lives between Glare 3-3/2-0.3 and 2024-T3 notched specimens at RT. Stresses in Glare are related to the aluminium layers, with and without the correction for anisotropy effects in the stress concentration factor.

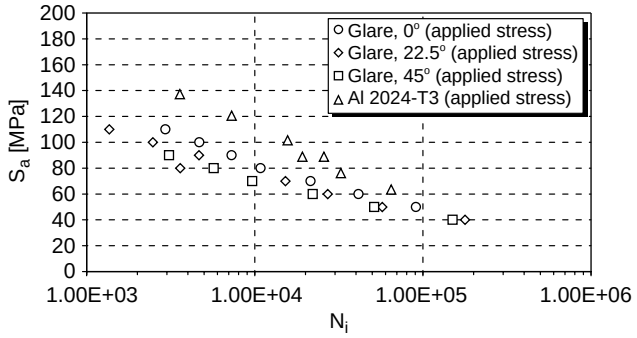


Fig. 11. Comparison of fatigue initiation lives between Glare 4B-3/2-0.3 under different off-axis angles and 2024-T3 laminates at RT. Stresses in Glare are related to the overall applied stresses.

substantially lower than those of the aluminium specimens if compared on the basis of the overall applied stresses. Further, it can be seen that there is a dependency on the load angle in Glare.

Looking to the comparison based on the stresses in the aluminium layers (Fig. 12), the test data of the Glare specimens with the 0° load angle show, just as for Glare 3, longer initiation lives than aluminium specimens. Test data of the Glare specimens with the 22.5 and 45° load angle show similar initiation lives as the aluminium specimens.

No correction is made based upon actual $K_t$ in a single aluminium layer in Glare because this $K_t$ is approximately 2.7 for all load angles, the same as for monolithic aluminium.

### 3.4. Effect of moisture and temperature

The effect of an exposure to a combination of moisture and elevated temperature (85% humidity, 70 °C, 3000 h) on the fatigue initiation behaviour is illustrated by Fig. 13. The choice of these environmental parameters was based on commonly used parameters for fibre reinforced plastics in aerospace industry. Tests were performed at RT on both exposed and unexposed notched specimens made of Glare 3-3/2-0.3. Fig. 13 shows that the exposure has not affected the initiation behaviour of Fibre Metal Laminates.

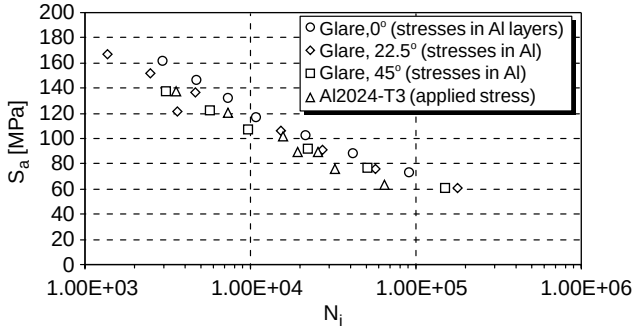


Fig. 12. Comparison of fatigue initiation lives between Glare 4B-3/2-0.3 under different off-axis angles and 2024-T3 laminates at RT. Stresses in Glare are related to the aluminium layers.

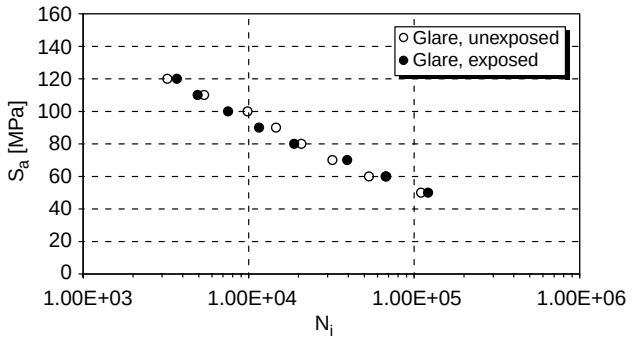


Fig. 13. Comparison of fatigue initiation lives between Glare 3-3/2-0.3 exposed (3000 h, 70 °C, 85% humidity) and unexposed. Stresses in Glare are related to the overall applied stresses.

It must be realized that tests were performed in an environment that did not change during the tests. Varying temperature, however, will lead to variations in the residual stress state of the FML and, therefore, introduce stress cycles which will have an effect on the fatigue behaviour of the FML.

## 4. Discussion and conclusions

Experiments showed that fatigue crack initiation in Fibre Metal Laminates is determined by the stress cycles in the metal layers only. Cycles to initiation ($N_i$) in Glare can be predicted as long as the actual stress levels in the metal layers are known. This is the case for both un-notched and notched specimens and for off-axis loading.

The internal stresses in the aluminium layers of a Fibre Metal Laminate are different from the applied stresses on the laminate because of differences in stiffness and coefficient of thermal expansion between the metal and fibre layers. Classical laminate theory has been applied to calculate the internal stresses. Additional elastic considerations have led to the means to account for the effect of anisotropy on the stress concentration factor.

Very often, the crack initiation life $N_i$ for monolithic aluminium is assessed using $S$–$N_f$ curves from the literature. Since the crack growth period has been neglected, this assessment will lead to errors. However, the crack growth period for monolithic material is relatively small and those errors are small as well. It is therefore, acceptable to use the same $S$–$N_f$ curves from the literature to assess the crack initiation life $N_i$ for Fibre Metal Laminates. Since Fibre Metal Laminates have a very long crack growth life, the method described in this paper cannot be used to estimate the fatigue life to failure $N_f$.

Experiments showed that exposure to a high temperature (70 °C) and humidity (85%) for 3000 h prior to testing has no effect on the fatigue initiation properties of Glare 3-3/2-0.3.

## Acknowledgements

Acknowledgments The author wishes to thank the Dutch National Aerospace Laboratories (NLR) and Mr Lambert Schra in particular for their cooperation.

## References

[1] Roebroeks GHJJ. Towards glare—the development of a fatigue insensitive and damage tolerant aircraft material. Doctor Thesis, Delft University of Technology, Faculty of Aerospace Engineering; 1991.
[2] Vlot A, Vogelesang LB. Towards application of fibre metal laminates in large aircraft. Aircraft Eng Aerosp Technol 1999;71:558–70.
[3] Vlot A, Gunnink JW, editors. Fibre metal laminates—an introduction. Kluwer Academic Publishers; 2001.
[4] Marissen R. Fatigue crack growth in ARALL, a hybrid aluminium–aramid composite material. Crack growth mechanisms and quantitative predictions of the crack growth rates, Report LR-574, Delft University of Technology, Faculty of Aerospace Engineering; 1988.
[5] Alderliesten RC. Development of an empirical fatigue crack growth prediction model for the Fibre Metal Laminate Glare. Master Thesis, Delft University of Technology, Faculty of Aerospace Engineering; 14 December 1999.
[6] Kieboom O. Fatigue crack initiation and early crack growth in Glare at different temperatures. Masters Thesis, Delft University of Technology, Faculty of Aerospace Engineering; November 2000.
[7] Lekhnitskii SG, Lekhnitskii SG. Anisotropic plates. Gordon and Breach; 1968.